PET Quantification of ^{18}F-Florbetaben Binding to β-Amyloid Deposits in Human Brains

Georg A. Becker*[1], Masanori Ichise*[2], Henryk Barthel[1], Julia Luthardt[1], Marianne Patt[1], Anita Seese[1], Marcus Schultze-Mosgau[3], Beate Rohde[3], Hermann-Josef Gertz[4], Cornelia Reininger[3], and Osama Sabri[1]

[1]*Department of Nuclear Medicine, University of Leipzig, Leipzig, Germany;* [2]*Columbia University, New York, New York;* [3]*Bayer Healthcare, Berlin, Germany; and* [4]*Department of Psychiatry, University of Leipzig, Leipzig, Germany*

^{18}F-florbetaben is a novel ^{18}F-labeled tracer for PET imaging of β-amyloid deposits in the human brain. We evaluated the kinetic model–based approaches to the quantification of β-amyloid binding in the brain from dynamic PET data. The validity of the practically useful tissue ratio was also evaluated against the model-based parameters. **Methods:** ^{18}F-florbetaben PET imaging was performed with concurrent multiple arterial sampling after tracer injection (300 MBq) in 10 Alzheimer disease (AD) patients and 10 age-matched healthy controls. Regional brain-tissue time–activity curves for 90 min were analyzed by a 1-tissue-compartment model and a 2-tissue-compartment model (2TCM) with metabolite-corrected plasma data estimating the specific distribution volume (V_S) and distribution volume ratio (DVR [2TCM]) and a multilinear reference tissue model estimating DVR (DVR [MRTM]) using the cerebellar cortex as the reference tissue. Target–to–reference tissue standardized uptake value ratios (SUVRs) at 70–90 min were also calculated. **Results:** All brain regions required 2TCM to describe the time–activity curves. All β-amyloid binding parameters in the cerebral cortex (V_S, DVR [2TCM], DVR [MRTM], and SUVR) were significantly increased in AD patients ($P < 0.05$), and there were significant linear correlations among these parameters ($r^2 > 0.83$). Effect sizes in group discrimination between 8 β-amyloid–positive AD scans and 9 β-amyloid–negative healthy control scans for all binding parameters were excellent, being largest for DVR (2TCM) (4.22) and smallest for V_S (3.25) and intermediate and the same for DVR (MRTM) and SUVR (4.03). **Conclusion:** These results suggest that compartment kinetic model–based quantification of β-amyloid binding from ^{18}F-florbetaben PET data is feasible and that all β-amyloid binding parameters including SUVR are excellent in discriminating between β-amyloid–positive and –negative scans.

Key Words: ^{18}F-florbetaben; ^{18}F-BAY 94-9172; ^{18}F-AV-1; Alzheimer disease; β-amyloid; compartment model; positron emission tomography; PET

J Nucl Med 2013; 54:723–731
DOI: 10.2967/jnumed.112.107185

Received Apr. 7, 2012; revision accepted Nov. 5, 2012.
For correspondence or reprints contact: Georg A. Becker, Department of Nuclear Medicine, University of Leipzig, Liebigstrasse 18, D-04103 Leipzig, Germany.
E-mail: georg.becker@medizin.uni-leipzig.de
*Contributed equally to this work.
Published online Mar. 7, 2013.

Several PET radiotracers that bind to β-amyloid deposits in the human brain are currently in research applications for the evaluation of Alzheimer disease (AD). After the successful introduction of Pittsburgh compound B, an ^{11}C-labeled tracer with a thioflavin-T–derived structure for β-amyloid PET imaging (*1–4*), fluorinated radiotracers have also been developed and successfully applied to image β-amyloid depositions in human brains. The half-life of ^{18}F (110 min) is approximately 5.5 times the half-life of ^{11}C, a great advantage in the routine clinical setting.

^{18}F-florbetaben (previously known as ^{18}F-BAY 94-9172 and ^{18}F-AV-1) is an ^{18}F-labeled stilbene derivative with high binding affinity (K_i = 6.7 nM) to postmortem human AD brain homogenates (*5*). Other ^{18}F-labeled PET radiotracers include the fluorinated Pittsburgh compound B derivative ^{18}F-flutemetamol (^{18}F-GE067) (*6,7*), the stilbene derivative ^{18}F-florbetapir (^{18}F-AV-45) (*8,9*), and the benzofuran radioligand ^{18}F-AZD4694 (*10*). ^{18}F-florbetapir was approved for clinical use by the U.S. Food and Drug Administration in April 2012 (*11*).

Early-phase clinical ^{18}F-florbetaben PET studies have demonstrated high diagnostic accuracy in the differentiation between AD patients and healthy controls (HCs) (*12,13*), as well as between AD patients and frontotemporal lobe degeneration (*14*). The utility of ^{18}F-florbetaben PET imaging was further confirmed by a recent multicenter phase 2 study that evaluated the sensitivity and specificity of ^{18}F-florbetaben PET in discriminating between probable AD patients (n = 81) and elderly HCs (n = 69), compared with clinical diagnosis (*15*).

In these studies, visual assessment or relative tissue ratio methods based on static PET images were used to assess ^{18}F-florbetaben binding to β-amyloid deposits in the brain. For example, the study by Barthel et al. (*13*) used a visual scoring system conducted by 3 independent masked readers and standardized uptake value ratios (SUVRs) of ^{18}F-florbetaben PET brain scans. That SUVR method used the radioactivity ratio of brain target regions containing β-amyloid deposits to reference tissue devoid of β-amyloid deposits (cerebellar cortex) measured at a fixed time interval after injection of the tracer. This relative quantitative

approach to quantify β-amyloid binding from static PET data is practical for routine clinical situations. However, according to the tracer kinetic compartment model theory for radiotracers such as ^{18}F-florbetaben that bind reversibly to the binding site in tissue, this tissue ratio reflects not only the available binding site density (B_{avail}) but also tracer delivery (blood flow) and tracer clearance to and from brain tissue (*16*). On the other hand, the kinetic model–based approaches for reversibly binding radiotracers may allow quantification of certain parameters that more directly reflect the binding density, although such approaches require dynamic PET data with or without serial arterial blood sampling.

The purpose of the present study was to evaluate the feasibility of kinetic model–based approaches to quantify β-amyloid binding parameters from dynamic PET data with or without blood data. The validity of the practically useful SUVR as a parameter of β-amyloid binding was also evaluated against the model-based binding parameters.

MATERIALS AND METHODS

Subjects

The subjects in the current kinetic modeling data analysis were from our phase 0 proof-of-mechanism trial (*13*) and consisted of 10 patients with AD (*17,18*) (mean age ± SD, 69 ± 7 y; Mini-Mental State Examination score, 19 ± 7; Clinical Dementia Rating score, 1–2) and 10 age-matched HCs (mean age, 67 ± 8 y; Mini-Mental State Examination score, ≥28; Clinical Dementia Rating score, 0). The local Institutional Review Board, the National Radiation Safety Committee, and the German Federal Institute for Drugs and Medical Devices approved the protocol, and written informed consent was obtained for all subjects involved in the study.

PET Image and Arterial Input Data Acquisition and Analysis

The florbetaben radiosynthesis, PET imaging, arterial sampling, and data processing were performed as recently described in detail elsewhere (*13,19*). In short, PET data were acquired with an ECAT HR+ scanner (Siemens/CTI) (*20*). ^{18}F-florbetaben was given over 90 s (300 ± 60 MBq). Four PET scans (29 frames) were acquired over 260 min (scan 1 lasting 90 min [23 frames] and scans 2, 3, and 4 starting at 2, 3, and 4 h [two 10-min frames per scan]). A preinjection transmission scan was obtained for attenuation correction. Thirty-four hand-drawn arterial samples were collected over 240 min after tracer injection. The portion of unmetabolized ^{18}F-florbetaben was determined by high-performance liquid chromatography, and the data points were fitted by a sum of 2 exponential functions. Because the plasma free fraction of the tracer was found to be smaller than 2% in preliminary samples and could therefore not be estimated with sufficient accuracy, no further plasma protein binding measurements were performed.

Dynamic PET data were motion-corrected and coregistered to the individual MR images. Volumes of interest were manually defined by an experienced neurobiologist in 13 brain regions with different volumes of interest for the left and right hemispheres when appropriate (Fig. 1). Time–activity curves for corresponding left and right brain structures were combined because our previous investigation (*13*) using standardized uptake values (SUVs) showed no significant differences between the left and right hemispheric regions. Time–activity curve data were expressed as SUV.

PET Data Analysis

After the preliminary kinetic data analysis of the entire dataset, in the current data analysis only 0- to 90-min dynamic data were used, for the following 2 reasons: first, beyond 90 min, head motion artifacts between scanning sessions cannot be completely excluded; and second, there were significant errors in the measurement of the metabolite-corrected arterial input function at late time points. PET data analysis was performed for regional time–activity curve data by compartmental models, a reference tissue model, and relative tissue ratios (SUVR), and these methods were compared. Additionally, voxelwise parametric images were generated using reference tissue models.

Compartmental Models

Kinetic analysis of regional time–activity curves was performed using 1- and 2-tissue-compartment models (1TCM and 2TCM, respectively). For the 2TCM, 2 differential equations describe the time course of nondisplaceable and specifically bound tracer concentrations in the target tissue (*16,21*):

$$\frac{dC_{ND}(t)}{dt} = K_1 C_P(t) - k_2 C_{ND}(t) - k_3 C_{ND}(t) + k_4 C_S(t) \quad \text{Eq. 1}$$

$$\frac{dC_S(t)}{dt} = k_3 C_{ND}(t) - k_4 C_S(t). \quad \text{Eq. 2}$$

$C_{ND}(t)$ is the nondisplaceable tracer concentration in the first tissue compartment, consisting of free tissue C_{FT}(t) and nonspecifically bound C_{NS}(t) radioactivity concentration, that is, $C_{ND}(t) = C_{FT}(t) + C_{NS}(t)$. The specifically bound tracer concentration in the second tissue compartment is $C_S(t)$ and the total tracer concentration $C_T(t) = C_{ND}(t) + C_S(t)$ (kBq·cm^{-3}).

Kinetic rate constants are K_1 (mL·cm^{-3}·min^{-1}), k_2 (min^{-1}), k_3 (min^{-1}), and k_4 (min^{-1}). K_1 describes tracer transport from arterial plasma into the first tissue compartment. k_2 describes transport from the first tissue compartment back into the blood pool. $k_3 = f_{ND} k_{on} B_{avail}$ describes binding of tracer to β-amyloid, where k_{on} (M^{-1}·min^{-1}) is the association rate constant for forming the complex of tracer and amyloid binding sites, B_{avail} (M) is the amyloid binding site density available for the tracer, and f_{ND} is the free tissue fraction of tracer in the nondisplaceable compartment, that is, $C_{FT}(t) = f_{ND} C_{ND}(t)$. The rate constant for dissociation of the β-amyloid tracer complex is given by $k_4 = k_{off}$. $K_D = k_{off}/k_{on}$ (M) is the equilibrium dissociation constant. The arterial input function corrected for metabolites $C_P(t)$ (kBq·mL^{-1}) consists of tracer free in plasma and bound to plasma proteins. The tracer concentration free in plasma water is given by $C_{FP}(t) = f_P C_P(t)$, with f_P being the free fraction in plasma.

By setting all derivatives in the differential equations (Eqs. 1 and 2) equal to zero, we can derive distribution volumes that describe the ratio of tissue to plasma concentration at equilibrium. The distribution volume of the first, nondisplaceable, compartment V_{ND} (mL·cm^{-3}) is given by

$$V_{ND} = \frac{K_1}{k_2} = \frac{C_{ND}^{eq}}{C_P^{eq}} = \frac{f_P}{f_{ND}} \frac{C_{FT}^{eq}}{C_{FP}^{eq}}, \quad \text{Eq. 3}$$

where the superscript eq denotes "at equilibrium." At equilibrium, $C_{FT}^{eq} = C_{FP}^{eq}$, and with Equation 3, the specific distribution volume V_S (mL·cm^{-3}) is given by

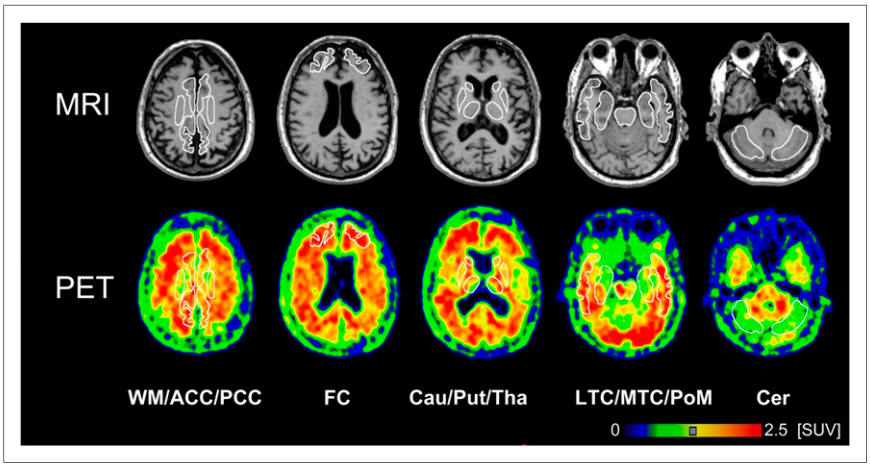

FIGURE 1. MR and ^{18}F-florbetaben PET images of β-amyloid binding with selected volumes of interest. Images were recorded from patient AD10 (62-y-old man) and summed over 60 to 90 min after injection. ACC = anterior cingulate cortices; Cau = nucleus caudatus; Cer = cerebellar cortices; FC = frontal cortices; LTC = lateral temporal cortices; MTC = mesial temporal cortices; PCC = posterior cingulate cortices; PoM = pons/midbrain; Put = putamen; Tha = thalamus; WM =white matter.

$$V_S = \frac{C_S^{eq}}{C_P^{eq}} = \frac{K_1 k_3}{k_2 k_4} = \frac{f_P B_{avail}}{K_D}. \quad \text{Eq. 4}$$

The total distribution volume V_T is

$$V_T = V_{ND} + V_S = \frac{K_1}{k_2}\left(1 + \frac{k_3}{k_4}\right) = \frac{K_1}{k_2}\left(1 + \frac{f_{ND} B_{avail}}{K_D}\right) = \frac{C_T^{eq}}{C_P^{eq}}, \quad \text{Eq. 5}$$

and the distribution volume ratio (DVR) can be computed according to

$$DVR = V_T/V_{ND} = C_T^{eq}/C_{ND}^{eq} = 1 + f_{ND} B_{avail}/K_D = 1 + BP_{ND}, \quad \text{Eq. 6}$$

where the binding potential (BP_{ND}) is

$$BP_{ND} = C_S^{eq}/C_{ND}^{eq} = DVR - 1. \quad \text{Eq. 7}$$

From Equations 4–7, V_S, BP_{ND}, and DVR (BP_{ND}+ 1) are the parameters that directly reflect the amyloid density B_{avail}.

Thus, using 2TCM, both receptor parameters, V_S (also called BP_P) and BP_{ND}, can be estimated. However, for many reversibly binding radiotracers, separate estimation of V_S and V_{ND} from the target time–activity curve data alone can be unreliable even when $V_T = V_S + V_{ND}$ is very reliable. If there is a brain region containing no target tissue (called the reference tissue) and if we can assume that V'_{ND} (prime denoting the reference tissue) in the reference tissue is equal to V_{ND} in the target tissue, we can replace V_{ND} by V'_{ND} to calculate V_S or BP_{ND}. In the current analysis, V_S and DVR were computed using the reference (cerebellar cortex) for the estimation of V'_{ND}.

There is an additional radioactivity concentration in the vascular space in tissue. The total PET signal is then described by

$$C_{PET}(t) = (1 - V_b) C_T(t) + V_b C_{WB}(t), \quad \text{Eq. 8}$$

where V_b is the vascular volume fraction of the whole blood activity concentration $C_{WB}(t)$. The parameter vector $\theta = [K_1, k_2, k_3, k_4, V_b]$ was estimated by minimizing the nonlinear least-squares cost function of the sum of squared differences between measured PET tracer concentrations and model predictions (*21,22*).

To compare the adequacy of data fitting between the 1TCM and the 2TCM, Akaike weights were used as a model selection criterion (*23*). DVR as opposed to BP_{ND} was chosen as a β-amyloid binding parameter because DVR is more directly comparable in magnitude to SUVR. DVR can also be estimated without blood data by reference tissue models. To distinguish the 2 DVRs, DVR estimated by 2TCM is abbreviated here as DVR (2TCM).

Reference Tissue Models

A multilinear reference tissue model (MRTM) was used to quantify DVR from the time–activity curve data (*24*). Here, DVR estimated by MRTM is abbreviated as DVR (MRTM) to distinguish it from DVR (2TCM). The operational equation for the MRTM is given by

$$C(T) = -\frac{V_T}{V'_T b}\int_0^T C'(t)dt + \frac{1}{b}\int_0^T C(t)dt - \frac{V_T}{V'_T k'_2 b} C'(T). \quad \text{Eq. 9}$$

This equation becomes linear after a certain time called t^*. $DVR = V_T/V'_T$ (MRTM) was estimated in MATLAB (version 7.3 [R2006b]; The MathWorks). DVR (MRTM) estimation was stable for t^* from 0 to 30 min. We set t^* equal to 10 min. Finally, SUVRs of target–to–cerebellar cortex regions obtained from a fixed interval at 70–90 min were calculated.

Comparison of β-Amyloid Binding Parameters

Mean β-amyloid binding and blood flow parameter values weighted for the size of the volume of interest and averaged over 4 cerebral cortical regions (frontal, lateral temporal, parietal and posterior cingulate cortices) were used to compare between β-amyloid binding–positive AD (n = 8) and β-amyloid binding–negative HC (n = 9) groups using the 2-tailed Student t test with Bonferroni adjustment for multiple comparisons when appropriate. These regions were chosen because they showed the highest β-amyloid deposition in the AD group (Fig. 2) and are known to be affected mainly in AD (*12,13*). "β-amyloid–positive" or "–negative" scans were defined as those scans visually interpreted unequivocally as positive or negative in our phase 0 proof-of-mechanism trial (*13*). The relationships between β-amyloid binding parameters by different models were evaluated by linear regression analysis, including all 11 cerebral cortical and subcortical brain regions excluding the white matter for all 10 AD and 10 HC subjects (n = 220 regions).

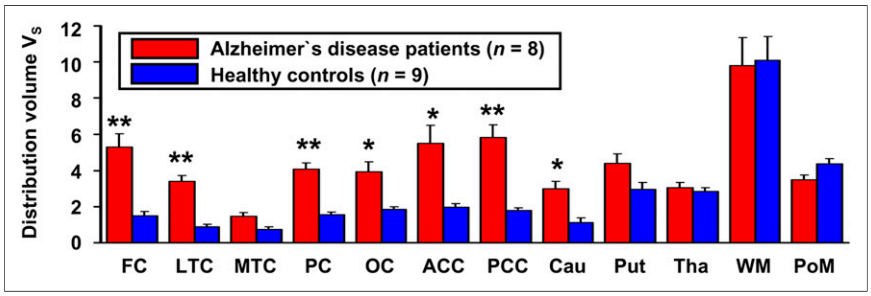

FIGURE 2. Graph showing significant increases of V_S in patients with AD in frontal (FC), lateral temporal (LTC), parietal (PC), occipital (OC), anterior cingulate (ACC), and posterior cingulate (PCC) cortices and head of caudate nucleus (Cau). No significant differences are seen in mesial temporal cortices (MTC), putamen (Put), thalamus (Tha), centrum semiovale (white matter, WM), and pons/midbrain (PoM). V_S is mean ± SEM for AD patients ($n = 8$) and HCs ($n = 9$). *$P < 0.05$. **$P < 0.002$.

Finally, to compare the ability of the 4 β-amyloid binding parameters (V_S, DVR [2TCM], DVR [MRTM], and SUVR) to distinguish between β-amyloid–positive AD ($n = 8$) and –negative HC ($n = 9$) scans, we evaluated the group effect size computed as the ratio of the difference between 2 means and the pooled SD, also called the Cohen *d* (*25*). Mean parameter values are expressed as mean ± SD or SEM in Figure 2.

Parametric Imaging of BP_{ND} and R_1

Voxelwise parametric images of BP_{ND} and relative blood flow ($R_1 = K_1/K_1'$) were also created using the reference tissue models, $MRTM_O$ and MRTM2 (*24*), implemented in PMOD (version 2.75; PMOD Technologies Ltd.). Here, BP_{ND} rather than DVR (MRTM) was chosen as a β-amyloid binding parameter because BP_{ND} parametric images show only BP_{ND}-positive voxels without any background signal, unlike original static PET images, and thus are suited for visual inspection of β-amyloid deposition patterns in the brain.

RESULTS

Compartmental Models

Figure 3 shows typical time–activity curves of ^{18}F-florbetaben in 1 HC and 1 AD patient. In the HC, both the frontal and the cerebellar cortices showed similar time–activity curve patterns, reaching peaks (3–4 SUVs) early within 10 min and showing rapid washout thereafter, whereas the white matter showed slow and lower uptake, reaching a peak (<2 SUVs) much later and showing much slower washout (Fig. 3B). On the other hand, in the AD patient, the frontal cortex time–activity curve reached a peak slightly later and washout was much slower than in the HC whereas the cerebellar cortex and white matter time–activity curves were similar to those of the HC (Fig. 3A). Thus, ^{18}F-florbetaben time–activity curves showed excellent reversible binding time–activity curve patterns.

All brain regions required the 2TCM to describe time–activity curves adequately. The fitting of the data was poor by the 1TCM (Fig. 4), and the Akaike weights used as a model selection criterion favored the 2TCM in all regions of all subjects. Therefore, 2TCM fitting was used for the subsequent analysis. The cerebral cortical vascular fraction V_b was approximately 0.04 in both the AD and the HC groups.

Table 1 shows examples of parameter values and coefficients of variation estimated by 2TCM for the frontal and cerebellar cortices of the same AD and HC subjects shown in Figures 3 and 4. K_1 and V_T values were well identified by 2TCM, with coefficients of variation being less than 6%.

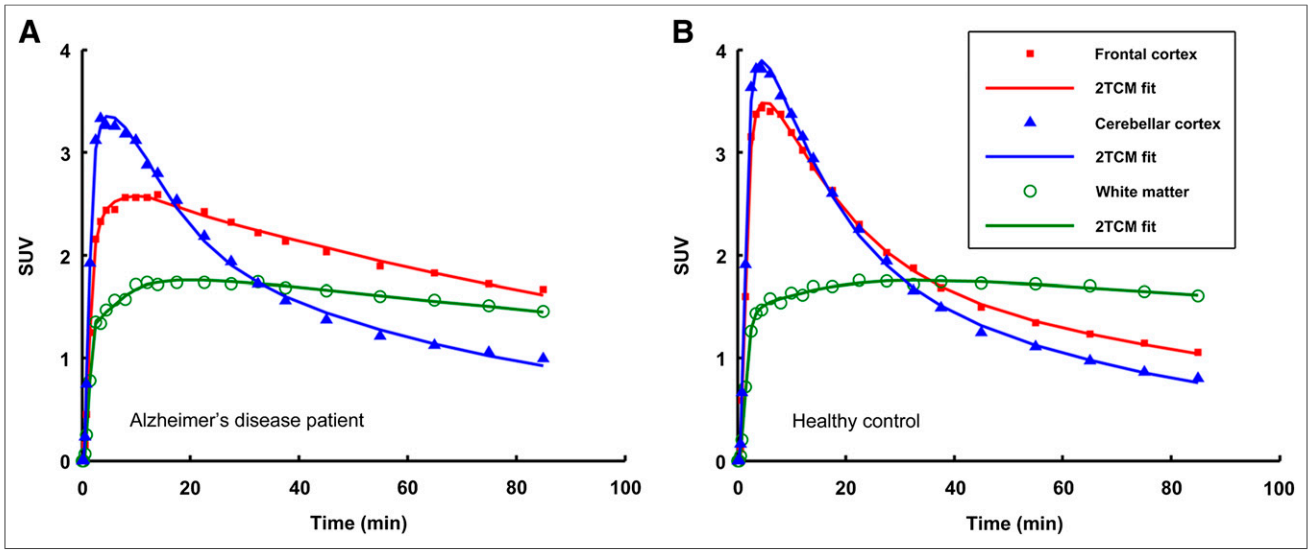

FIGURE 3. 2TCM fits of measured time–activity curves for frontal cortex, cerebellar cortex, and white matter in AD patient (A) and HC (B).

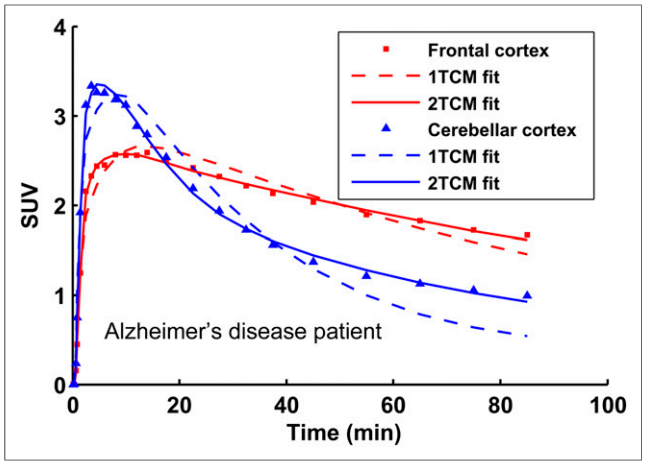

FIGURE 4. Time–activity curves fitted with 1TCM and 2TCM for frontal and cerebellar cortices of AD patient.

The other parameters (k_2, k_3, and k_4) were also relatively well identified, with the coefficients of variation of k_3 being largest, at around 15%.

Group mean values (8 β-amyloid–positive AD patients and 9 β-amyloid–negative HCs) of average parameter values of the 4 cerebral cortical regions and the cerebellar cortex are listed in Table 2. The mean cortical V_S values were about 3 times higher in the AD group than in the HC group ($P < 10^{-4}$). On the other hand, the mean K_1 values, which reflect regional blood flow, were significantly lower in the AD group than in the HC group ($P < 0.005$). However, as expected, there were no significant differences in mean K_1' values or V_T' values for the cerebellar cortex between the AD and HC groups ($P > 0.3$) (Table 2).

Figure 2 compares V_S in all individual brain regions between the AD and HC groups. The mean V_S values were significantly higher in the AD group than in the HC group in all brain regions ($P < 0.05$, uncorrected for multiple comparisons) except in the thalamus and white matter (centrum semiovale), where there were no differences ($P > 0.9$) between the 2 groups. After the correction for multiple comparisons, the mean V_S values in the mesial temporal cortex ($P = 0.07$), putamen ($P = 0.47$), and pons/midbrain ($P = 0.53$) did not reach statistical significance. However, the mean V_S values in the 4 cortical regions (frontal, lateral temporal, parietal, and posterior cingulate cortices) ($P < 0.002$) all were markedly higher (2.01–9.75 mL/cm^3 for AD patient vs. 0.36–2.43 mL/cm^3 for HC), with the highest V_S values in the posterior cingulate cortex/precuneus (3.64–9.75 mL/cm^3). The mean V_S values were also higher, albeit to a mild degree, in the occipital and anterior cingulate cortices and in the head of the caudate nucleus in the AD group than in the HC group ($P < 0.05$) (Fig. 2).

Reference Tissue Models

Both the group mean DVR (MRTM) and SUVRs averaged over 4 cortical regions were significantly higher in the AD group than in the HC group (AD: DVR = 1.54 ± 0.07 and SUVR = 1.79 ± 0.14; HC: DVR = 1.18 ± 0.11 and SUVR = 1.30 ± 0.12) ($P < 10^{-4}$) (Table 2).

Comparison of β-Amyloid Binding Parameters

The mean values for DVR (MRTM) in 11 cerebral cortical and subcortical brain regions in each hemisphere excluding the white matter (1.36 ± 0.25) for 10 AD patients and 10 HC subjects were 8% lower than those for DVR (2TCM) (1.47 ± 0.30) ($P < 0.05$). However, there was a strong linear relationship between the 2 sets of DVRs ($r^2 = 0.83$, $P < 10^{-4}$) (Fig. 5A). The corresponding mean SUVRs (1.52 ± 0.32) were 3% higher than the mean DVR (2TCM) values (1.47 ± 0.30) ($P < 0.05$). However, there was also a strong linear relationship between the 2 sets of SUVRs and DVR (2TCM) values ($r^2 = 0.85$, $P < 10^{-4}$) (Fig. 5B). Finally, the mean SUVRs (1.52 ± 0.32) were 12% higher than the mean DVR (MRTM) values (1.36 ± 0.25) and there was also a strong linear relationship between the SUVRs and DVR (MRTM) values ($r^2 = 0.90$, $P < 10^{-4}$) (Fig. 5C).

Figure 6 illustrates individual plots of β-amyloid binding parameters for the average of 4 cortical regions between 10 AD patients and 10 HC subjects. The effect size in comparing between the 8 amyloid-positive AD scans and 9

TABLE 1
Kinetic Parameters by 2TCM Fit for 1 AD and 1 HC Subject

Parameter	Frontal cortex		Cerebellar cortex	
	AD	HC	AD	HC
K_1 (mL·cm^{-3}·min^{-1})	0.187 (2.0)	0.216 (1.0)	0.275 (1.8)	0.251 (1.3)
k_2 (min^{-1})	0.076 (12.7)	0.0845 (3.3)	0.090 (6.7)	0.100 (3.9)
k_3 (min^{-1})	0.117 (14.1)	0.024 (9.0)	0.037 (15.3)	0.022 (12.7)
k_4 (min^{-1})	0.0258 (7.0)	0.013 (13.8)	0.023 (14.0)	0.019 (15.1)
V_T (frontal cortex) and V_T' (cerebellar cortex)	13.7 (2.8)	7.22 (5.6)	7.85 (4.2)	5.36 (4.2)
$V_S = V_T - V_T'$	5.85	1.86		

Data are parameter values and percentage SE of parameter estimation by 2TCM in parentheses. This SE is given for each cortical region. Time–activity curves of the 2 subjects are given in Figures 3 and 4.

TABLE 2
Comparison of β-Amyloid Binding and Blood Flow Parameters Between β-Amyloid–Positive AD (n = 8) and –Negative HC (n = 9) Groups

Parameter	Mean values of 4 cortical regions*			
	AD	HC	Cohen *d*	*P*
2TCM				
K_1 (mL·cm^{-3}·min^{-1})	0.195 ± 0.019	0.246 ± 0.037	NA	0.003
V_T (mL·cm^{-3})	10.62 ± 2.57	6.84 ± 1.07	NA	0.001
K_1' (mL·cm^{-3}·min^{-1})	0.252 ± 0.018	0.281 ± 0.070	NA	0.28
V_T' (mL·cm^{-3})	6.05 ± 1.24	5.45 ± 1.13	NA	0.32
$V_S = V_T - V_T'$ (mL·cm^{-3})	4.57 ± 1.44	1.38 ± 0.47	3.25	<0.0001
DVR (2TCM)	1.75 ± 0.13	1.27 ± 0.11	4.22	<0.0001
Reference tissue models				
DVR (MRTM)	1.54 ± 0.067	1.18 ± 0.11	4.03	<0.0001
SUVR	1.79 ± 0.14	1.30 ± 0.12	4.03	<0.0001

*Frontal, lateral temporal, parietal, and posterior cingulate cortices.
NA = not applicable.
Data are expressed as mean ± SD. Effect size in group comparison was determined by Cohen *d,* and *P* values were calculated by Student *t* test (2-tailed, unpaired).

amyloid-negative HC scans calculated as Cohen d values (the higher values indicating the better group discrimination) were largest for DVR (2TCM) (4.22) and smallest for V_S (3.25), and they were intermediate and the same for DVR (MRTM) and SUVR (4.03) (Table 2). The 4 amyloid binding parameters showed no overlap between amyloid-positive AD patients and amyloid-negative HCs (Fig. 6).

Parametric Imaging of BP_{ND} and R_1

Examples of transaxial parametric images of BP_{ND} and corresponding R_1 at a mid-thalamic level for selected subjects (2 different AD subjects, AD1 and AD2, and 1 HC subject) are shown in Figure 7. BP_{ND} images clearly showed β-amyloid binding in the frontal and temporal cortices in the 2 AD subjects but only the white matter signal with no cerebral cortical β-amyloid binding in the HC subject. The corresponding R_1 images on the other hand showed decreased relative blood flow, particularly in the posterior temporal lobes, in the AD subjects compared with the HC subject. BP_{ND} and R_1 are 2 independent parameters. For example, BP_{ND} is increased in regions where R_1 is decreased in the temporal lobes whereas BP_{ND} is only minimally increased or nearly zero in regions where R_1 is not decreased. Our preliminary visual inspection of BP_{ND} parametric images showed that these images were easier to interpret than corresponding static original images.

DISCUSSION

^{18}F-florbetaben and ^{18}F-florbetapir have recently undergone phase 3 clinical trials including postmortem histologic investigations of β-amyloid deposits in the brain of subjects who underwent PET imaging with these tracers. ^{18}F-florbetapir PET images and the rating of postmortem results (positive or negative) for β-amyloid agreed in 96% of 29 individuals who underwent the scan within 1 y before death (*8*). For routine clinical studies, it would be most practical to perform static PET imaging at a fixed time after injection of the tracer. We found that both compartment model–based β-amyloid binding parameters and the practically useful tissue ratios at a fixed time after tracer injection are excellent in discriminating between β-amyloid–positive and –negative scans. Of several ^{18}F-labeled β-amyloid compounds that have been examined in vivo, ^{18}F-flutemetamol and ^{18}F-AZD4694 have also been examined using a compartment analysis with arterial input function to validate the use of tissue ratios (*6,10*).

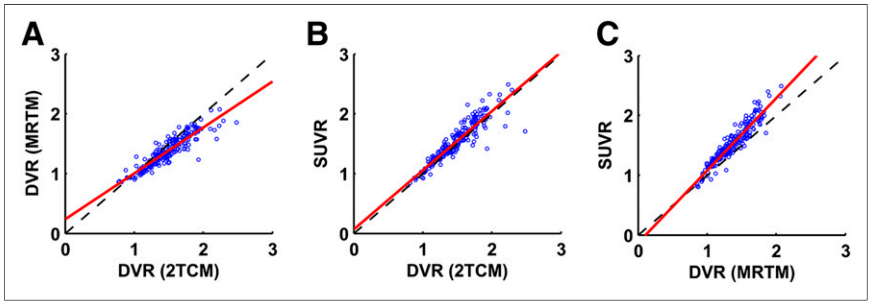

FIGURE 5. Linear regression analysis. (A) DVR computed by DVR (MRTM) and DVR (2TCM), $y = 0.768x + 0.234$, $r^2 = 0.832$. (B) SUVR and DVR (2TCM), $y = 0.988x + 0.068$, $r^2 = 0.846$. (C) SUVR and DVR (MRTM), $y = 1.209x - 0.127$, $r^2 = 0.898$.

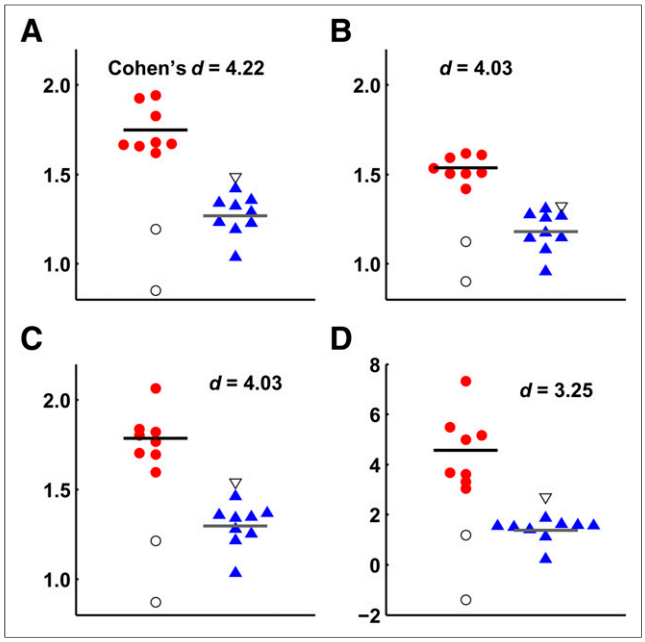

FIGURE 6. Individual plots of β-amyloid parameters in β-amyloid–positive (8 AD patients, ●) and –negative (9 HCs, ▲) subjects. Two AD patients (○) and 1 HC (△) were excluded from statistical analysis because they were scored by 3 masked readers as β-amyloid–negative and –positive, respectively. Effect size in group comparison was determined by Cohen *d,* and subfigures are presented in decreasing order of Cohen *d* values: DVR (2TCM) (A), DVR (MRTM) (B), SUVR (C), V_S (D).

^{18}F-florbetaben kinetics in the cortical and subcortical brain regions except in the white matter were relatively fast both in AD patients and HCs, with time–activity curves peaking quickly (<10 min) and showing relatively quick washout thereafter within the 90-min scan (Figs. 3 and 4). Although we performed PET imaging over 240 min in this phase 0 study in which we did not have a priori knowledge of the kinetics of ^{18}F-florbetaben in the human brain, we chose to analyze only time–activity curves of continuously acquired 90-min data because of the logistic limitation inherent in the data beyond 90 min.

Although the regional tracer delivery rate constant K_1 was relatively high (0.2–0.25 mL·cm^{-3}·min^{-1}) (Table 2), regional brain uptake was relatively low (<4 SUVs at peak) (Figs. 3 and 4). This relatively low brain uptake, which is also found in all other β-amyloid tracers (*3,6,10*), may be explained by the fact that the free plasma fraction of ^{18}F-florbetaben is low ($f_P < 0.02$) (as described in "Materials and Methods"), although measurements of the free plasma fraction have not been reported for any other β-amyloid tracers.

Both β-amyloid parameters—V_S and DVR (2TCM)—are linearly proportional to the β-amyloid binding site density B_{avail} (Eqs. 4 and 6). The differences between the 2 parameters relate to the 2 different additional constants, f_P for V_S and f_{ND} for DVR (2TCM). In terms of the effect size in discriminating between β-amyloid–positive and –negative scans, DVR (2TCM) (Cohen $d = 4.22$) was slightly superior to V_S (Cohen $d = 3.22$). This slight superiority of DVR (2TCM) over V_S may be due to the group differences in the plasma free fraction of the tracer, f_P. V_S can be made independent of f_P by normalizing it by f_P. However, f_P was very low, and we could not measure it accurately.

V_S can be estimated from target time–activity curve and blood data without the reference tissue data (Eq. 5). This approach requires estimation of V_{ND} separately (Eq. 3). In our study, V_{ND} was linearly correlated with K_1 whereas $V_T = V_{ND} + V_S$ or V_T' was not significantly correlated with K_1 or K_1'. Therefore, we used V_T' as the estimate of the nondisplaceable distribution volume in target regions as done for many other reversibly binding tracers.

In the present study, compartment kinetic analysis required a 2TCM to describe the reference tissue. We carefully created cerebellar regions of interest to exclude spillover of activity from the adjacent white matter. Thus, the effect of spillover, if any, would have been minimal and would be unlikely to account for the 2TCM kinetics because the 1TCM fitting was clearly inferior to 2TCM fitting. All 3 other tracers examined using compartment analyses (*3,6,10*) showed 2TCM kinetics in the cerebellar cortex, including ^{11}C-Pittsburgh compound B (*3*), which is known to show less white matter binding. These 2TCM kinetics in the cerebellar cortex might be due to the existence of a slow nonspecific binding compartment in the cerebellar cortex. Another potential issue regarding the

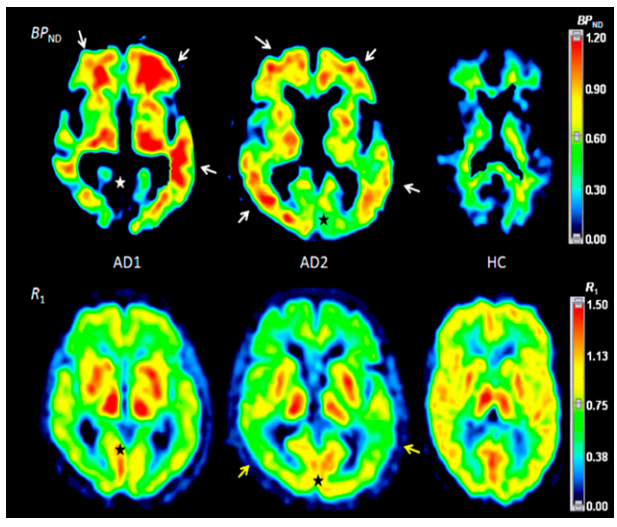

FIGURE 7. Parametric images of BP_{ND} (DVR − 1) (top row) and corresponding R_1 (bottom row) generated by MRTMs ($MRTM_O$ and MRTM2, respectively). BP_{ND} images clearly show β-amyloid binding in frontal and temporal cortices in 2 AD subjects (white arrows) but only white matter signal with no cerebral cortical β-amyloid binding in HC subject (top right). Corresponding R_1 images show decreased relative blood flow, particularly in posterior temporal lobes in AD subjects (yellow arrows) compared with HC subject. BP_{ND} and R_1 are 2 independent parameters. For example, BP_{ND} is increased (white arrows) in regions where R_1 is decreased (yellow arrows) in temporal lobes, whereas BP_{ND} is only minimally increased or nearly zero in regions where R_1 is not decreased (stars).

use of the cerebellar cortex relates to the known presence of β-amyloid deposits in the cerebellar cortex in familial AD. The pons has been suggested as an alternative reference tissue (*26*). This alternative approach will need to be carefully evaluated for ^{18}F-florbetaben in the future.

Compartmental model–based reference tissue models including MRTM allow for the estimation of BP_{ND} and DVR (MRTM) without blood data. These parameters are linearly proportional to B_{avail} and do not depend on f_P but on a different constant, f_{ND}, the free tissue fraction. DVR (MRTM) is given by the ratio V_T/V_T', although separate estimation of individual distribution volumes is not possible without blood data. Theoretically, therefore, DVR (2TCM) and DVR (MRTM) in the present study are identical parameters. DVR (MRTM) was 8% lower than DVR (2TCM), with a strong linear relationship between the 2 DVRs. The MRTM parameter estimation is known not to be significantly affected by the presence of noise in the PET data (*24*). However, the underestimation of DVR (MRTM) may be due to the fact that both the target and the reference region were described by 2TCM (*24*).

Practically useful and simple-to-calculate SUVR was an excellent β-amyloid parameter with a strong linear relationship between SUVR and DVR (2TCM), although SUVR slightly overestimated DVR (2TCM) by 3%. This excellent SUVR performance suggests that at around 90 min after injection, the tracer kinetics of ^{18}F-florbetaben may be at so-called transient or pseudo equilibrium, a situation in which the SUVR is known to be overestimated (*27*). However, the pseudo equilibrium time point can be affected by changes in blood flow and tracer clearance. In the same individual at different times, such as 6 mo later after therapy, regional brain blood flow and kidney function may change significantly and SUVR from a follow-up scan performed at a fixed time after injection may be significantly altered even if there are no significant interval changes in the β-amyloid status. Therefore, in selected research studies evaluating, for example, the efficacy of a new drug for AD, DVR (MRTM) or BP_{ND} would be more appropriate. Further evaluations of the parameter performance in such situations appear warranted.

Finally, parametric images of BP_{ND} and R_1 were generated from dynamic PET data using reference tissue models in the present study. The 2-parameter version of MRTM (MRTM2) allows for the voxelwise fitting of dynamic PET data to generate BP_{ND} and R_1 relatively unaffected by noise in the voxel PET data (*24*). BP_{ND} parametric images would be useful for the visual assessment of β-amyloid binding. BP_{ND} images show a prominent signal in the white matter that contains no β-amyloid deposits (Fig. 7). The exact cause of this peculiar high nonspecific binding of β-amyloid binding tracers in general is not known. R_1 images appear to reflect relative blood flow (Fig. 7); these images can readily be coregistered onto MR images, and coregistered BP_{ND} MR images can readily be generated using the same R_1–to–MR-image transformation matrix.

CONCLUSION

Compartment kinetic model–based quantification of β-amyloid binding from ^{18}F-florbetaben PET data is feasible, and all β-amyloid binding parameters, including those by the reference tissue model and the practically useful SUVR, are excellent in discriminating between β-amyloid–positive and –negative scans.

DISCLOSURE

The costs of publication of this article were defrayed in part by the payment of page charges. Therefore, and solely to indicate this fact, this article is hereby marked "advertisement" in accordance with 18 USC section 1734. This trial was supported by Bayer Healthcare (Berlin, Germany). Drs. Sabri, Barthel, and Ichise received consultant honoraria from Bayer Healthcare. Drs. Sabri, Barthel, Ichise, and Becker received speaker and travel honoraria from Bayer Healthcare. Drs. Rohde, Reininger, and Schultze-Mosgau are employees of Bayer Healthcare. No other potential conflict of interest relevant to this article was reported.

ACKNOWLEDGMENTS

We thank all patients, their caregivers, and the healthy volunteers who participated in this trial. We are also grateful to the cyclotron, radiochemistry, and PET imaging staff of the Department of Nuclear Medicine, University of Leipzig (Germany), for their excellent technical assistance.

REFERENCES

1. Klunk WE, Engler H, Nordberg A, et al. Imaging brain amyloid in Alzheimer's disease with Pittsburgh compound-B. *Ann Neurol.* 2004;55:306–319.
2. Rowe CC, Ng S, Ackermann U, et al. Imaging β-amyloid burden in aging and dementia. *Neurology.* 2007;68:1718–1725.
3. Price JC, Klunk WE, Lopresti BJ, et al. Kinetic modeling of amyloid binding in humans using PET imaging and Pittsburgh compound-B. *J Cereb Blood Flow Metab.* 2005;25:1528–1547.
4. Klunk WE, Mathis CA. The future of amyloid-beta imaging: a tale of radionuclides and tracer proliferation. *Curr Opin Neurol.* 2008;21:683–687.
5. Zhang W, Oya S, Kung MP, Hou C, Maier DL, Kung HF. F-18 polyethyleneglycol stilbenes as PET imaging agents targeting Aβ aggregates in the brain. *Nucl Med Biol.* 2005;32:799–809.
6. Nelissen N, Van Laere K, Thurfjell L, et al. Phase 1 study of the Pittsburgh compound B derivative ^{18}F-flutemetamol in healthy volunteers and patients with probable Alzheimer disease. *J Nucl Med.* 2009;50:1251–1259.
7. Vandenberghe R, Van Laere K, Ivanoiu A, et al. ^{18}F-flutemetamol amyloid imaging in Alzheimer disease and mild cognitive impairment: a phase 2 trial. *Ann Neurol.* 2010;68:319–329.
8. Clark CM, Schneider JA, Bedell BJ, et al. Use of florbetapir-PET for imaging β-amyloid pathology. *JAMA.* 2011;305:275–283.
9. Joshi AD, Pontecorvo MJ, Clark CM, et al. Performance characteristics of amyloid PET with florbetapir F 18 in patients with Alzheimer's disease and cognitively normal subjects. *J Nucl Med.* 2012;53:378–384.
10. Cselényi Z, Jonhagen ME, Forsberg A, et al. Clinical validation of ^{18}F-AZD4694, an amyloid-β-specific PET radioligand. *J Nucl Med.* 2012;53:415–424.
11. FDA approves ^{18}F-florbetapir PET agent. *J Nucl Med.* 2012;53(6):15N.
12. Rowe CC, Ackerman U, Browne W, et al. Imaging of amyloid β in Alzheimer's disease with ^{18}F-BAY94-9172, a novel PET tracer: proof of mechanism. *Lancet Neurol.* 2008;7:129–135.
13. Barthel H, Luthardt J, Becker G, et al. Individualized quantification of brain β-amyloid burden: results of a proof of mechanism phase 0 florbetaben PET trial in patients with Alzheimer's disease and healthy controls. *Eur J Nucl Med Mol Imaging.* 2011;38:1702–1714.

14. Villemagne VL, Ong K, Mulligan RS, et al. Amyloid imaging with ^{18}F-florbetaben in Alzheimer disease and other dementias. *J Nucl Med.* 2011;52: 1210–1217.
15. Barthel H, Gertz HJ, Dresel S, et al. Cerebral amyloid-β PET with florbetaben (^{18}F) in patients with Alzheimer's disease and healthy controls: a multicentre phase 2 diagnostic study. *Lancet Neurol.* 2011;10:424–435.
16. Innis RB, Cunningham VJ, Delforge J, et al. Consensus nomenclature for in vivo imaging of reversibly binding radioligands. *J Cereb Blood Flow Metab.* 2007; 27:1533–1539.
17. American Psychiatric Association. *DSM-IV: Diagnostic and Statistical Manual of Mental Disorders*. 4th ed. Washington, DC: American Psychiatric Association; 1994:143–147.
18. McKhann G, Drachman D, Folstein M, Katzman R, Price D, Stadlan EM. Clinical diagnosis of Alzheimer's disease: report of the NINCDS-ADRDA Work Group under the auspices of Department of Health and Human Services Task Force on Alzheimer's Disease. *Neurology.* 1984;34:939–944.
19. Patt M, Schildan A, Barthel H, et al. Metabolite analysis of [^{18}F]florbetaben (BAY 94-9172) in human subjects: a substudy within a proof of mechanism clinical trial. *J Radioanal Nucl Chem.* 2010;284:557–562.
20. Brix G, Zaers J, Adam LE, et al. Performance evaluation of a whole-body PET scanner using the NEMA protocol. *J Nucl Med.* 1997;38:1614–1623.
21. Bertoldo A, Cobelli C. Physiological modelling of positron emission tomography images. In: Carson E, Cobelli C, eds. *Modelling Methodology for Physiology and Medicine*. San Diego, CA: Academic Press; 2001:179–211.
22. Carson RE. Parameter estimation in positron emission tomography. In: Phelps ME, Mazziotta JC, Schelbert HR, eds. *Positron Emission Tomography and Autoradiography: Principles and Applications for the Brain and Heart*. New York, NY: Raven Press; 1986:347–390.
23. Burnham KP, Anderson DR. *Model Selection and Multimodel Inference: A Practical Information Theoretic Approach*. 2nd ed. New York, NY: Springer-Verlag; 2002:70–75.
24. Ichise M, Liow JS, Lu JQ, et al. Linearized reference tissue parametric imaging methods: application to [^{11}C]DASB positron emission tomography studies of the serotonin transporter in human brain. *J Cereb Blood Flow Metab.* 2003;23:1096–1112.
25. Hartung J, Knapp G, Sinha BK. *Statistical Meta-Analysis with Application*. Hoboken, NJ: Wiley; 2008:13–22.
26. Knight WD, Okello AA, Ryan NS, et al. Carbon-11-Pittsburgh compound B positron emission tomography imaging of amyloid deposition in presenilin 1 mutation carriers. *Brain.* 2011;134:293–300.
27. Carson RE, Channing MA, Blasberg RG, et al. Comparison of bolus and infusion methods for receptor quantitation: application to [^{18}F]cyclofoxy and positron emission tomography. *J Cereb Blood Flow Metab.* 1993;13:24–42.